Spatial analysis of an elephant mass mortality event: investigating the role of cyanobacteria blooms in the Okavango's waterholes

Davide Lomeo,[1*] Emma J. Tebbs,[1] Nlingisisi D. Babayani,[2] Michael A. Chadwick,[1] Mangaliso J. Gondwe,[2] Anne D. Jungblut,[3] Graham P. McCulloch,[4] Eric R. Morgan,[5] Daniel N. Schillereff,[1] Stefan G. H. Simis,[6] Anna C. Songhurst[4]
* Corresponding Author

[1] Department of Geography, King's College London, London, United Kingdom.
[2] Okavango Research Institute, University of Botswana, Maun, Botswana.
[3] Department of Life Sciences, Natural History Museum, London, United Kingdom.
[4] Ecoexist, Maun, Botswana.
[5] School of Biological Sciences, Queen's University, Belfast, United Kingdom.
[6] Plymouth Marine Laboratory, Plymouth, United Kingdom.

- Davide Lomeo* - davide.lomeo@kcl.ac.uk
- Emma J. Tebbs - emma.tebbs@kcl.ac.uk
- Nlingisisi D. Babayani - NBabayani@ub.ac.bw
- Michael A. Chadwick - michael.chadwick@kcl.ac.uk
- Mangaliso J. Gondwe - mgondwe@UB.AC.BW
- Anne D. Jungblut - a.jungblut@nhm.ac.uk
- Graham P. McCulloch - gmc.ocb@gmail.com
- Eric R. Morgan - Eric.Morgan@qub.ac.uk
- Daniel N. Schillereff - daniel.schillereff@kcl.ac.uk
- Stefan G. H. Simis - stsi@pml.ac.uk
- Anna C. Songhurst - fielddirector@ecoexistproject.org

* Corresponding Author

Abstract

The 2020 mass mortality of 350 African elephants (*Loxodonta africana*) in the Okavango Delta, Botswana sparked global concern. These deaths have been tentatively linked to cyanotoxins in watering holes (pans), but evidence remains inconclusive. In this study, we used remote sensing in combination with spatial analysis to explore the relationship between the ecohydrology of ~3,000 pans and the locations of deceased elephants. Our findings reveal a significant difference in the spatial distribution of fresh versus decayed elephant carcasses ($p < 0.001$), suggesting that the die-off event deviated from characteristic, regional patterns of elephant deaths. From our analysis we identified 20 pans near the sites of fresh carcasses that experienced increased phytoplankton (microalgae or cyanobacteria) bloom events in 2020 ($n = 123$) compared to the previous 3 years combined ($n = 23$). Additionally, these pans in 2020 also exhibited the highest average phytoplankton biomass of the period 2015 - 2023 (Normalised Difference Chlorophyll Index > 0.2; $p < 0.001$). These findings suggested an elevated risk and higher likelihood of cyanotoxins presence in these pans. Our spatial analysis also demonstrated that elephants walked an average of 16.5 km (± 6.2 km) and died within 88 hours (± 33 hours) from initial exposure, offering metrics that were previously unknown for these elephants. Our study presents important evidence that cyanobacterial toxicity could be a factor in the 2020 mass die-off, while also considering other possible causes. Moreover, we highlight the necessity of integrating spatial analysis and ecohydrological assessments to inform conservation strategies to potentially mitigate future mortality events.

Introduction

The 2020 die-off of 350 elephants in Botswana was one of the biggest mortality events of large wild mammals in southern Africa in recent years [1]. The remote location in the north-eastern sector of Botswana known as the eastern Okavango Panhandle, and timing at the peak of the COVID-19 pandemic, hindered attempts to respond to and investigate the event [2]. Although this area is a known poaching hotspot in Botswana [3], this was ruled out since elephant carcasses were found with tusks intact [4]. Other initial theories included virulent and bacterial causes, such as encephalomyocarditis virus or anthrax, but evidence from the field, such as the age of dead elephants, and the absence of clinical signs, deemed both unlikely [5]. The cause of the die-off has later been officially attributed by the Government of Botswana to environmental intoxication by cyanobacterial toxins, also known as cyanotoxins[6].

Cyanobacteria are a group of benthic or planktonic phototrophic prokaryotes often abundant in turbid, stagnant, and nutrient-rich waters, and several bloom-forming species can cause harm due to the production of toxins [7]. Evidence suggests that phytoplankton (microalgae or cyanobacteria) blooms, events in which population size increases exponentially due to favourable conditions [8], are becoming more frequent worldwide due to increased anthropogenic nutrient input and climate change [9]. Links between harmful blooms and animal mortality events are well represented in literature, including cyanotoxin poisoning [10,11]. Cyanobacteria are a common occurrence in water bodies in southern Africa [12,13], and have previously been linked to wildlife mortality events [14].

The Okavango Delta is hydrologically complex and characterised by permanent and ephemeral waterbodies filled by seasonal flooding or local rainfall alongside the river itself and associated lakes. A recent study has revealed increased cyanobacteria bloom occurrences in perennial lakes within the Okavango Delta in 2020[15], suggesting cyanotoxins as a possible cause of death of the elephants. However, new evidence of *Pasteurella* sp. in carcasses arisen from a die-off event of elephants in the neighbouring Zimbabwe in 2020, suggest that this bacterium may have been the cause of the mass mortality event in Botswana[16]. Unfortunately, as the event occurred in an especially remote location hard to sample logistically, during movement restriction due to the COVID-19 pandemic, comprehensive in situ water and tissue samples contemporary with the die-off have not been collected. Moreover, there is currently a lack of knowledge on the condition of waterholes (or pans) in the eastern Okavango Panhandle, directly where the die-off occurred, which would elucidate on the possibility of cyanobacteria involvement in the die-off.

In the absence of solid outbreak sample data, we explore an alternative strategy to reconstruct elephants' travel ranges in relation to the location and conditions of pans in the eastern Okavango Panhandle. This work applies an extensive spatial analysis on elephant carcasses locations recorded during an aerial survey after the mortality event [17], together with satellite-derived location and conditions of pans in the region. In particular, the Automated Water Extraction Index (AWEI)[18] was used to indicate the location and water availability of pans, while the Normalised Difference Chlorophyll Index (NDCI) [19] was used as a proxy for phytoplankton biomass in pan water. The generic NDCI is used as an indicator of biomass concentrations because other diagnostic alternatives that provide concentration estimates in mg m^{-3} do not exist for such small and shallow waterbodies. Noting that cyanotoxins are not directly detectable from space, the presence and abundance of cyanobacteria, especially if bloom-forming, which is known to be dominant in regional pans[20,21], can increase the likelihood of cyanotoxin production and accumulation.

This approach not only circumvents logistical challenges but also provides a scalable model for investigating wildlife mortality events in similarly inaccessible regions. This work addresses a crucial gap in understanding the spatial-temporal relationship between pan conditions and elephant deaths. We investigate whether the proximity of carcasses to pans with suspected phytoplankton bloom activity corroborates the hypothesis that deteriorating water quality has caused the die-off. Our results contribute to elucidating the causes behind such mass mortality events and demonstrate the utility of incorporating spatial analysis and remote sensing into routine wildlife health monitoring. This approach enhances wildlife conservation efforts and informs public health strategies, providing vital insights for potentially preventing and controlling future incidents.

Results

Spatial analysis of elephant carcasses and live elephants

The mass mortality event in Botswana occurred in the eastern Okavango Panhandle region within the concession areas NG11, NG12, and NG13, in the north-easternmost sector of the Okavango Delta (Fig. 1). The area is enclosed by veterinary fences to the north (a double border fence with Namibia) and a 'buffalo fence' to the east and south. These fences were originally installed to prevent the transmission of infectious diseases from wild animals to domestic animals, like the foot and mouth disease carried by buffalos [22], and lung disease in cattle [23]. An aerial survey carried out in mid-July 2020 to investigate the event using a small aircraft [17] revealed 161 fresh carcasses (estimated from their state of decomposition to have been dead less than 6 months; named carcasses hereafter), 222 old carcasses (dead between 6 months and 10 years; bones hereafter), and 2,682 live elephants across the area [24]. The dead elephants were of varying age, with tusks intact, and no carcasses of other wildlife or livestock species were observed at the time of the survey. We used bones as an indication of what a 'normal' or 'natural' distribution of carcasses across the eastern Okavango Panhandle is expected to be, whereas we assumed that carcasses with skin were very recent thus associated with the die-off event.

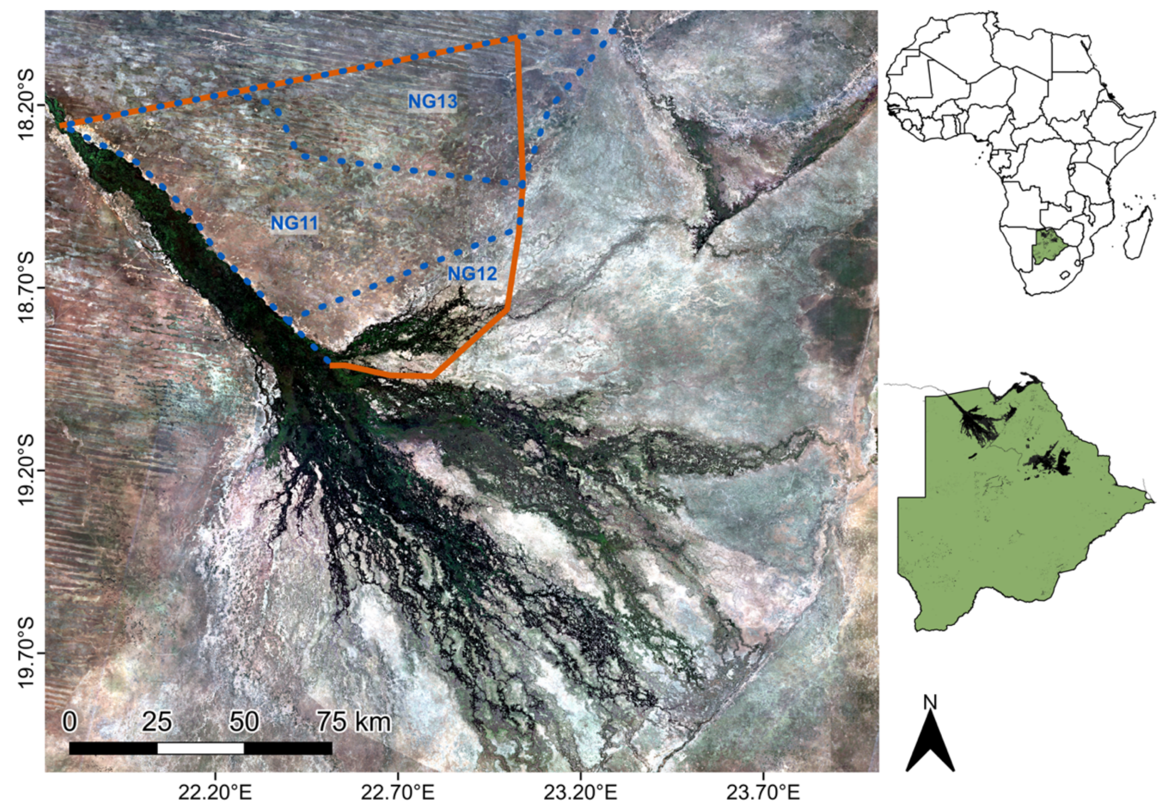

Figure 1 | The eastern Okavango Panhandle area in northern Botswana and the veterinary fence enclosing it. The satellite image on the left shows the Okavango Delta, located in the north of Botswana, in May 2020. The image was captured by Sentinel-2 Multispectral Instrument in the period 15-31/05/2020, at Level-2A (surface reflectance). The blue dotted lines show the boundaries of the concession areas NG11, NG12 and NG13. The orange lines show the boundaries of the veterinary fence that runs along the border with Namibia in the north. The green shape to the right shows the territory of Botswana, and the black areas within it are areas where water is regularly detected.

The spatial distribution of elephant carcasses significantly differed from that of bones and live elephants, with carcasses notably closer to pans (Two-Samples Kolmogorov-Smirnov test, KS test, $p < 0.001$; Supplementary Table 1). Specifically, live elephants were mainly observed in dry woodlands, particularly in the NG11 and NG13 sectors of the eastern Panhandle, and dispersed across the NG12 area, near the Okavango Delta wetland system and along the 'buffalo' veterinary fence (Fig. 2). In contrast, bones were scattered more broadly across the landscape, covering an area of approximately 6,500 km², with notable concentrations near the eastern Panhandle's wetlands. Carcasses, however, were primarily found in a more confined area (~4,350 km²), considerably distant from the wetlands and human settlements. Our analysis revealed significant differences in the proximity of each elephant category to water sources (KS test, $p < 0.001$). Carcasses were, on average, located closer to pans (1,635 m ± 2,317 m) compared to bones (4,545 m ± 3,477 m) and live elephants (5,672 m ± 3,814 m). Distinct clustering patterns emerged among the categories. Live elephants exhibited the most pronounced clustering, followed by carcasses, then bones. This variance was statistically significant (KS test, $p<0.001$), highlighting different spatial behaviours and associations. Specifically, bones showed the greatest number of clusters (n = 14), indicative of widespread dispersion, followed by live elephants (n = 13), and carcasses (n = 5), with the average number of individuals per cluster being substantially higher for carcasses (n = 29 ± 54) than for bones (n = 11 ± 11) or live elephants (n = 9 ± 5). Notably, a significant portion of the carcasses were found within a single cluster (n = 126), hinting at a common underlying cause for these deaths. Given these results, we decided to focus the remainder of the analysis solely on the location of the fresh carcasses arisen from the die-off.

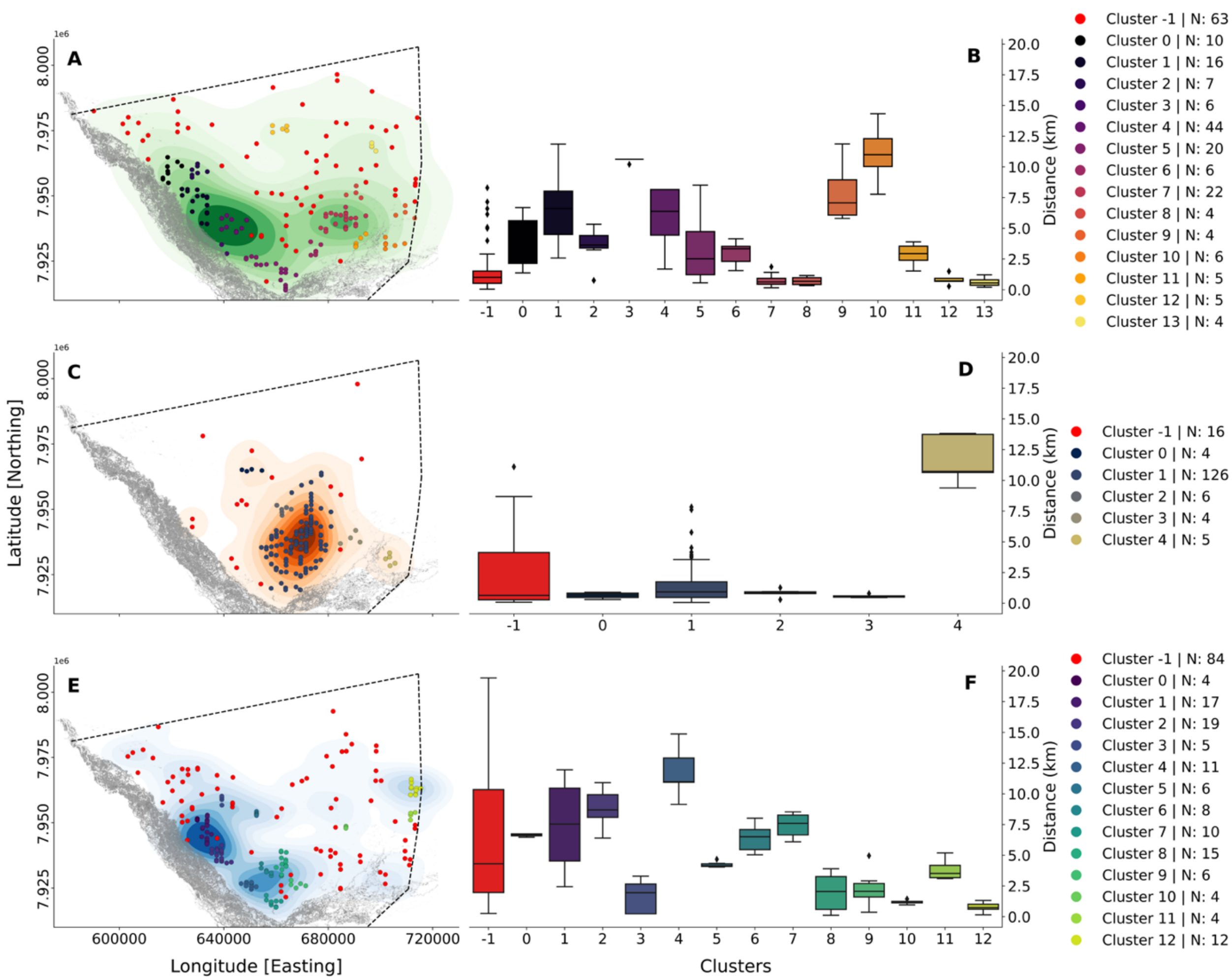

Figure 2 | Clustering of bones, fresh carcasses, and live elephants, and distances to nearest pans. Panels A, C and E show the distribution of bones, fresh carcasses, and live elephants across the eastern Okavango Panhandle, respectively. The shadings around the points represent the kernel density estimates of their distributions, and their colour weight is gradually more intense towards areas of higher concentrations of points. The dotted black lines represent the veterinary fence. Panels B, D and F show boxplots of distances between individual bones, carcasses, and live elephants belonging to different clusters and the nearest pan, respectively. For bones and carcasses, we used the location of pans detected by Sentinel-2 Multispectral Instrument (MSI) in April 2020 (i.e., peak of wet season in 2020). For live elephants we used the location of pans detected by MSI at the time of the aerial survey (July 2020). Clusters numbered as -1 and coloured in red in the maps and in the boxplots are groups of points that are not statistically significant in the overall dispersion of the three categories ($p > 0.05$). These points do not belong to any cluster and are not included in the analysis. The points in panels A, C, and E, are coloured such that they match the colour of the cluster they belong to in the boxplots in panels B, D and F, respectively. The legends to the right of the image refer to the panels in the same row, and 'N' refers to the number of individuals belonging to each cluster.

Ecohydrology of pans and climate

We identified 3,389 unique pans in the eastern Okavango Panhandle, and examination of their ecohydrology revealed a major shift in water availability and phytoplankton growth between 2019 and 2020. This suggests potential implications for water quality, which may have impacted local wildlife. Using imagery from the Sentinel-2A/B Multispectral Instrument (MSI) from August 2015 to September 2023, we observed strong interannual fluctuations in the number of pans. The highest number of pans was observed in 2021 (n = 3,389), while the lowest was recorded in 2016 (n = 724) (not considering 2015, for which image collection started from August). We employed Moran's I local spatial association statistic to identify pans spatially related with the central locations of carcass clusters, rather than with individual positions (Supplementary Fig. 1). This approach assumes that elephants dying within the same cluster would have faced similar environmental influences from nearby water sources. By analysing cluster centres, we were able to narrow our study to a set of 1,232 pans spatially related to carcasses cluster centres. We conducted a temporal analysis on these pans to assess changes in Normalised Difference Chlorophyll Index (NDCI), used as a proxy for phytoplankton biomass, and Automated Water Extraction Index (AWEI), used as a proxy of water availability, alongside precipitation and temperature data. The data was converted into bi-weekly averages to reduce noise and account for varying satellite overpass (3-5 days), as well as missing images due to cloud cover. NDCI exhibited consistently high values since 2020, contrasting with more variable pre-2020 levels (Fig. 3). AWEI values showed a dramatic increase in water availability from 2020 onwards, diverging from consistently low levels before 2019. Contextualising these findings against background environmental conditions, we found that 2019 had one of the lowest precipitation levels in the period 2010-2023 and followed by a wet 2020. Temperature in 2019 was much higher than the 2010-2023 average and followed by a relatively cooler 2020. Pans in proximity to carcass cluster centres revealed that a marked increase in water availability coincided with sustained high phytoplankton biomass, as evidenced by post-2019 NDCI. The drastic changes in ecohydrological and climate conditions, particularly in the shift between 2019 (i.e., notably low rainfall and high temperatures) and 2020 (i.e., high rainfall and lower temperature), underscore the likelihood for altered water quality and increased harmful cyanobacteria bloom risks. These environmental dynamics, occurring in tandem with the carcass spatial clustering, provide compelling evidence of water quality deterioration as a possible contributing factor in the mass die-off event.

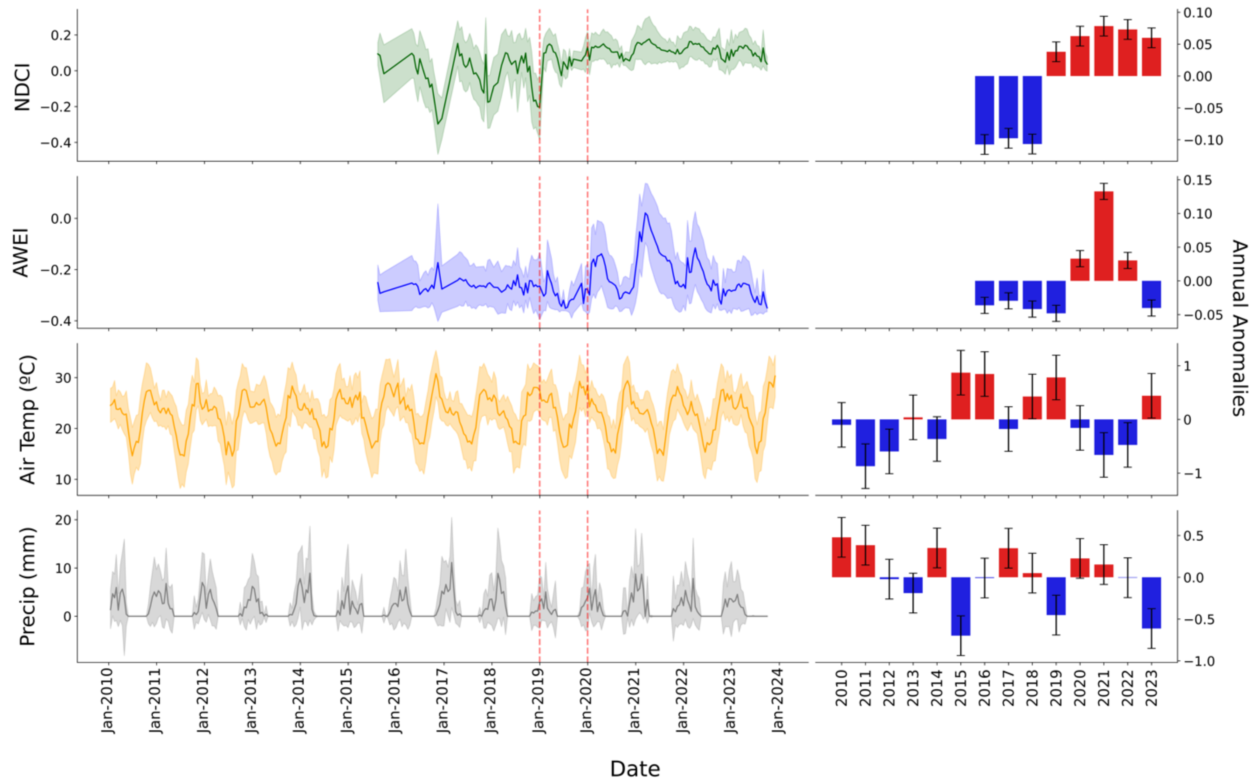

Figure 3 | Algal biomass and water availability of pans spatially associated to fresh elephant carcasses alongside air temperature and precipitation. The four panels on the left show the bi-weekly averages of the Normalised Difference Chlorophyll Index (NDCI), the Automated Water Extraction Index (AWEI), air temperature and precipitation, from top to bottom, respectively. The two vertical dotted lines are positioned between January 2019 and January 2020 to highlight the ecohydrological and climatic condition in the Eastern Okavango Panhandle region in the year preceding the mass mortality event. The four bar plots on the right show the anomalies between the 'long-term' averages of NDCI, AWEI, air temperature, and precipitation, and their annual averages, respectively, from top to bottom. The long-term averages for NDCI and AWEI were calculated from the period 2016 – 2023, limited by Sentinel-2 Multispectral Instrument observations, which started in August 2015. The long-term averages for air temperature and precipitation were calculated from the period 2010 – 2023.

Distance covered by elephants before death

Toxicological timelines of cyanotoxin-related animal deaths in the literature[10] suggest an association between animal size and time of death, the latter occurring between 15 minutes and 120 hours (hrs) after initial exposure (Supplementary Table 2). Most of these studies focus on dogs, cattle, and sheep, with some instances of wildlife reporting like deer and rhinoceros. Extrapolating these findings to elephants, we looked at potential timeframes of 24, 48, 72, 96, 120, and 144 hrs. We then calculated feasible travel ranges using the average speed of 4.5 km per day in this area [25] (Supplementary Fig. 2) to give potential distances between cyanotoxin exposure and death. Furthermore, since the potential distances were calculated concentrically from the cluster centres, we integrated three standard deviation ellipses [26] from cluster centres to account for the directional distribution of the carcasses. This was based on the premise that elephants do not move in a single direction throughout the day [27] and to weigh-in the arrangement of carcasses across the landscape. By considering areas shared by all circular distances and standard deviation ellipses, noting the relatively even spread of carcasses across these areas, we estimated that elephants may have walked an average of 16.5 km (±6.2 km) after initial exposure to harmful cyanobacteria blooms and cyanotoxins and could have died within 88 hrs (±33 hrs).

Potential sources of the die-off

To indicate high phytoplankton biomass for pans in the region we used a threshold of NDCI = 0.3. We obtained this figure by adding the mean and standard deviation (SD) of NDCI of all previously identified 1,232 pans between Aug 2015 and Sep 2023 for each timestamp (i.e., bi-weekly averages), and pulled the maximum value from the upper SD. Additionally, to identify bloom events we arbitrarily used an increase of NDCI = 0.1 between consecutive timestamps. Using these metrics, we further narrowed the 1,232 pans spatially associated to carcass cluster centres to a set of 151 pans. These pans where within the identified elephants' area of travel, that either showed NDCI > 0.3 or experienced sharp NDCI increases (0.1 units) between consecutive timestamps, or both, at least once in 2020 (Supplementary Table 3). These 151 pans were all spatially associated with the largest cluster of carcasses (cluster 1; Fig. 2 C and D). These pans showed repeated high phytoplankton biomass events, with NDCI values up to 0.5, especially in the period 2020 and 2021. The period between April and May 2020 showed the highest algae production, although highly productive pans and bloom events were recorded throughout the year. On average, these pans had water in the period Jan-Jul 2019 only 11% of the time, compared to 55% during the same period in 2020.

To find the most likely sources of poisoning within the elephants' area of travel, we used the same NDCI thresholding described earlier on the 151 pans, specifically looking for pans that experienced repeated (more than twice) high phytoplankton biomass events in 2020, pinpointing 20 pans. Satellite observations revealed that most of the 20 pans were either completely dry prior to 2020, or too small to be detected using MSI images, with a few exceptions (Fig. 4). These pans showed unprecedented phytoplankton biomass between March and May 2020, when elephants were recorded to have died in large numbers. Visual validation of SuperDove images at 3 m spatial resolution confirmed that these pans exhibited repeat blooms between April and May 2020, at different times and intensities (Supplementary Fig. 3). During this period, the size of these 20 pans ranged between 2 and 22 km^2, demonstrating how bloom events occurred irrespective of size or water availability. SuperDove images also revealed that the landscape surrounding these pans was highly heterogeneous, with no obvious links between land cover types around pans and bloom events. Finally, we found that the average distance of these 20 pans from the centre of cluster 1 was 11.6 km (±5.2 km), which aligns with the estimated distance walked by elephants before dying.

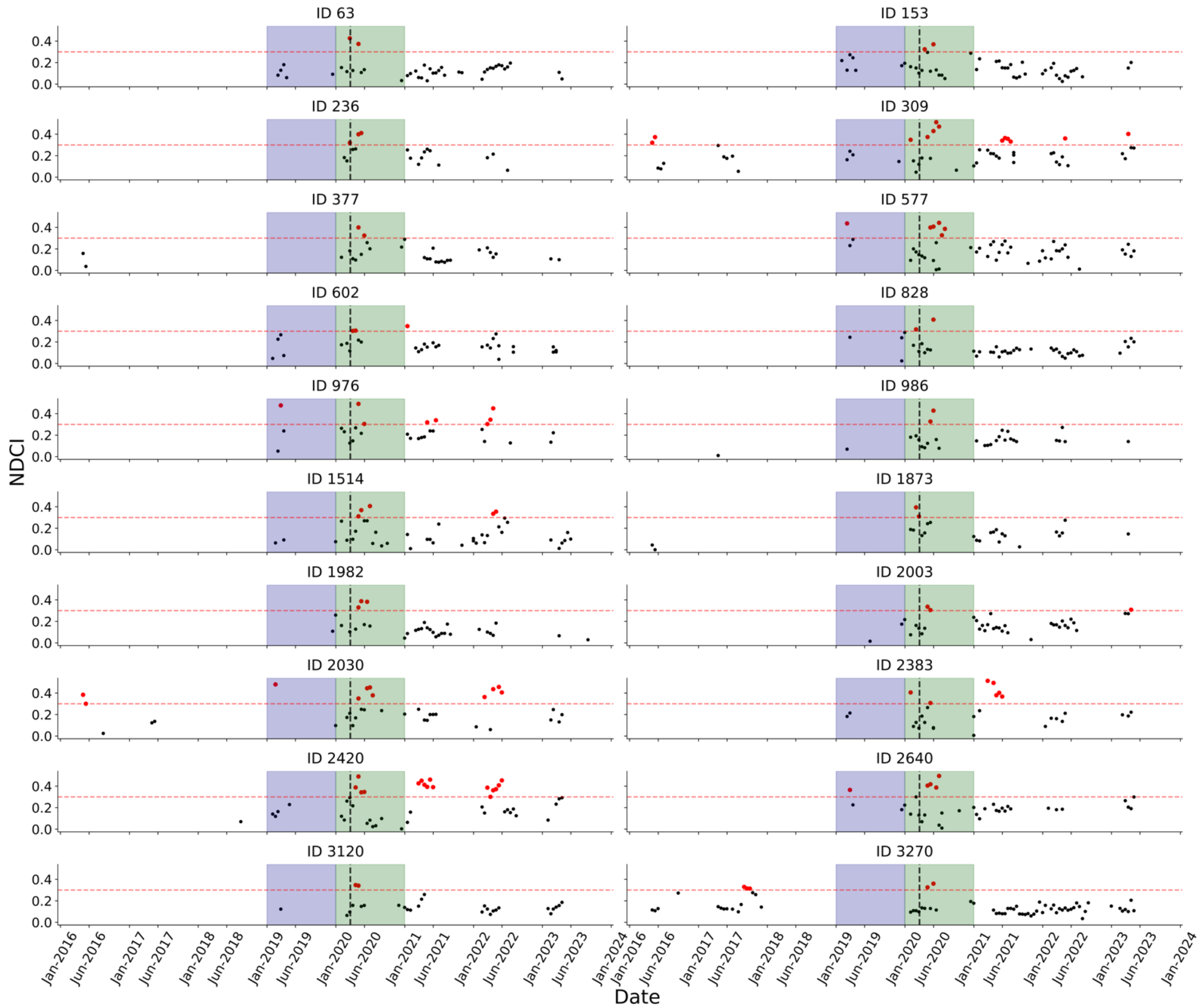

Fig. 4. **NDCI timeseries of the twenty pans in eastern Okavango Panhandle that showed the highest algal biomass activity in 2020.** Some of the pans show no points prior 2019 because they were likely dry, or too small to be detected using Sentinel-2 Multispectral instrument images. The horizontal red dotted line is placed on NDCI = 0.3 to show the maximum upper-end NDCI average value across 1,232 pans between Aug 2015 and Sep 2023 used in the analysis as a threshold to highlight high phytoplankton biomass events. Red dots are single observations (pans) when NDCI was >= 0.3, whereas the vertical black dotted line aligns with the time of first elephant death reporting (18/03/2020 [28]). Areas shaded in blue and green correspond to the 12 months in 2019 and 2020, respectively.

Discussion

This study investigated the 2020 elephant die-off event in the eastern Okavango Panhandle in Botswana using an extensive spatial analysis of the carcass locations in concert with a remote sensing assessment of water quality in pans. By comparing the locations of carcasses and elephant bones and linking locations to the ecohydrology of the thousands of pans in the study region we provide new evidence to support the likelihood that deaths may be linked to cyanotoxin poisoning. Our results highlight that seasonal, predominantly rain-fed pans, rather than the permanent waterbodies (i.e., rivers and lagoons) within the Panhandle, were the likely source of cyanotoxin exposure. Pans in close proximity to the carcasses showed elevated phytoplankton biomass and repeated bloom events in 2020 compared to previous years, particularly during the period associated with the mass mortality event [2], increasing the likelihood of cyanotoxin accumulation in pan water.

Live elephants were mostly found near the Okavango Delta because in the dry month of July they move there for water and to forage [29]. Some elephants clustered along the veterinary fence probably because it acts as a physical barrier that prevents them from ranging further [30]. Elephant bones representing deaths in previous years were, in contrast to fresh carcasses, more spread out across the landscape, as demonstrated by the high number of spatial clusters over a wider area (Fig. 2), indicative of a weaker spatial relationship between these points. Some points associated with relatively high numbers of individuals were found nearer the Okavango Delta, but it is challenging to know the cause without relevant data. One likely cause may be mortality from human-elephant conflict, indicated by their proximity to human settlements and the associated increased mortality risk for elephants, owing to high human-elephant competition for shared space and resources in this area of the eastern Okavango Panhandle [31]. Heightened competition for space and resources often leads to problematic animal control mortalities [32] and sometimes increases the risk of poaching [33]. However, predation and natural causes leading to accumulations of bones cannot be ruled out.

Fresh elephant carcasses, on the other hand, were predominantly distributed in a region far from the Okavango River and Delta and human settlements. These carcasses were more densely clustered than bones, indicating that the cause of death was likely localised in this area (Fig. 2). The higher proximity of fresh carcasses to pans compared to bones may be due to seasonality, since at the time of high elephant mortality in 2020, towards the end of the wet season, elephants tend to stay closer to pans with water [27]. The fact that the average distance between carcasses and the nearest pans was lower than bones (Fig. 2 D) could also be linked to an observed altered behaviour of sick elephants roaming closer to water sources [34,35]. Nonetheless, this spatial pattern is also consistent with water in pans as the source of any potential cyanotoxin poisoning. The additional temporal relationships with phytoplankton biomass, such that clustering of fresh carcasses was associated with specific overgrowth events, provides compelling evidence for a causative link, rather than elephants being drawn to water in general, and in contrast to reporting of algal bloom anomalies in the wider region [15]. The strong clustering of carcasses also suggests that the event was sudden, with limited dispersal of elephants prior to death. Notably, a single cluster of carcasses (cluster 4, Fig. 2 D) was found much further from the others. These elephants may have been part of the same herd, but moved towards this area while sick and their movement was later limited by the standing waters in the Okavango Delta.

Water availability was a major issue in the eastern Okavango Delta in 2019, when it was at its lowest level of the past 8 years (Fig. 3). This was likely driven by lower-than-average precipitation between Oct 2018 and Mar 2019, and higher-than-average temperature in May-Sep 2018. This is particularly relevant for the pans close to the sites of fresh carcasses since these are far from the Okavango Delta and are primarily filled by rain or groundwater, normally recharged by floods, thereby contributing to the observed patterns [36]. Lack of precipitation and higher temperatures have led to the drying of most pans between 2018 and 2019, and long-standing stagnant waters, where available, likely promoted increased phytoplankton activity. Cyanobacteria are frequently abundant in turbid, nutrient-rich waters [7], and tend to dominate these types of water over other phytoplankton species [8]. We theorise that the shift from such a dry 2019 and an extremely wet 2020 may have led to a resuspension of significant amounts of sediments and nutrients, both from the previously dry beds of the pans and the surrounding soil, promoting unprecedented productivity in 2020.

The process of nutrients release through sediment resuspension is known [37], and has been documented for the seasonally dry wetlands of the Okavango Delta [38]. Pans that were either completely dry or with little water left in 2019 experienced a dramatic volume of water delivered by rainfall, directly exposing them to sediment resuspension and the associated nutrient release. It is important to state that this process does not affect waterbodies equally, even if very similar in principle and surrounded by the same landscape, and that the release of nutrients and consequent eutrophication are system-dependent[37]. This variability emphasises the need for individual pan analysis in our research, to avoid assuming uniform ecological dynamics across neighbouring pans. Residual cyanotoxins might have persisted in the pans from previous years as shown for deserts' soil crusts [39–41], and there is a possibility that those produced prior to 2020 may have remained in the pans' dried-up bed soil and resuspended in the water. Furthermore, cyanobacteria cells deposited in the sediment from previous years might have inoculated pans' water and increases chances of bloom formation.

Unsurprisingly, April and May were the months with the highest frequency of bloom events in 2020. This period is at the end of the rainy season when rainfall drastically decreases and temperature start rising. Thus, standing water in pans remain relatively undisturbed, presenting the ideal conditions for cyanobacterial growth. The analysis shows that 2015 was also a very dry year (Fig. 3), but the following 2016 rainy season did not deliver the same volumes of water of 2020, which may explain why such sustained phytoplankton biomass levels were not observed then. Although our analysis of water presence and quality in pans is limited to the period 2015-2023, a recent study has shown that 2019 was the driest year of the past two decades in the region[42]. The resuspension processes and related nutrient increase in pans we describe, coupled with the unprecedented succession of events between 2019 and 2020, could explain why a mortality event of this size was yet to be recorded in Botswana in the scientific literature.

An understanding of the spatial-temporal dynamics is essential for determining the movement patterns of elephants in response to cyanotoxin exposure. We estimated that elephants may have walked an average of 16.5 km (± 6.2 km) before dying within approximately 88 hrs (±33 hrs) and this aligns with reported toxicological timelines for other large mammals[10]. It is worth noting that the approach to establishing the distance walked by elephants before dying is not based on observed elephant movement, since it is challenging to determine movement behaviours from point analysis, and noting that elephants do not move in a single direction throughout the day[25,27]. Therefore, the analysis is not intended to inform on walking behaviours of elephants after initial potential exposure to cyanotoxins. Instead, it attempts to estimate the potential distances that elephants may have walked before dying, and possibly the time it may have taken them to die after initial (or repeated) cyanotoxin ingestion based on the distribution of the carcasses.

By analysing bloom dynamics in the pans spatially associated with carcasses cluster centres, we pinpointed 20 locations that experienced extremely frequent and severe bloom events of different magnitudes during the critical period between April and May 2020 (Fig. 4). These pans were all spatially associated to cluster 1, the cluster with the largest number of individuals (Fig. 2, D), and were all located an average of 11.6 km (±5.2 km) from the centre of the cluster. This figure aligns with the estimated distance walked by elephants before dying, making these pans strong candidates as the potential sources of the intoxication. These pans were of various sizes and surrounded by different types of landscapes (Supplementary Fig. 3), so it is challenging to determine what may have made them particularly susceptible to bloom events.

Since cyanotoxins are not directly detectable from space, it is not possible to determine which pans contained lethal concentrations and for how long. Nevertheless, prolonged, and repeated algal bloom events increase the likelihood of cyanotoxins in the water, provided the presence of toxin-producing strains of cyanobacteria[43], which have been already observed in this part of the world [44]. Since elephants can drink between 100 to 200 L of water per day, depending on temperatures [45–47], it is highly likely that they drank from multiple pans before their death. It cannot be established if the fatal intoxication occurred in a single drinking event, but it seem more plausible that if cyanotoxins were present and were the cause of the die-off, this was through toxins bioaccumulation in elephants' organs [48].

The recent finding of *Pasteurella* spp. in elephant carcasses in Zimbabwe [16] has shed light on the possibility of African elephants to contract this bacterial infection in Botswana also, although it remains uncertain what may have led to its development and transmission [16]. It is possible that elephants in the eastern Okavango Panhandle contracted and spread the disease, leading to the disruption of their immune systems, altered movement, and sensitivity to other mortality factors. Ingestion of higher concentrations, or more potent, cyanotoxins from water compared to 'normal' levels may conversely have led to higher susceptibility to other bacteria, including *Pasteurella* spp., leading to their death. The association between cyanobacterial intoxication and the presence of *Pasteurella multocida*, has previously been reported in a study that found traces of *Pasteurella* in various internal organs of flamingo carcasses arisen from a mortality event in Tanzania [49]. This is not an exhaustively comparable study but raises questions on our current understanding of the interplay between cyanobacteria and other bacteria species, including *Pasteurella*.

Unfortunately, we do not have evidence from the ground to corroborate either *Pasteurella* spp., cyanotoxins, or a given species of cyanobacteria, or other diseases as the dominant cause. Our evidence shows that, at the very least, mortality was highly localised near water sources of suspect quality, from currently available remote sensing methods. Future launch of high spatial resolution sensors (order of 1-10 m) equipped with diagnostic wavebands for cyanobacteria pigment (around 620 nm), like those on current medium resolution (300 m) ocean colour sensors, would contribute greatly to diagnosing cyanobacteria dynamics in these ecosystems. Other causes, including poaching, have been previously ruled out [5], and the analysis shows that water was widely available in the eastern Okavango Panhandle in 2020. Hence, death by lack of water (or drought), which has historically led to multiple elephant mass mortality events in Africa [50–52], does not seem plausible given the presence of water throughout the region at the time of the event.

The drinking behaviour of elephants might have played a role in their susceptibility to cyanotoxins, as drinking depth and timing might impact cyanotoxin intake due to cyanobacterial aggregation influenced by density variations, photosynthetic cycles, and environmental factors[53,54]. This can lead to different toxin concentrations at various water layers, which elephants may be more likely to encounter. Differently from other species that drink from the side of pans, elephants wade into the middle of the waters to drink[55], with the potential of disturbing benthic mats[56] or causing planktonic biomass to sink and accumulate at the bottom. This behaviour, coupled with the way elephants submerge their trunk to drink, can expose elephants to higher concentrations of cyanotoxins[55]. While our research primarily focuses on planktonic cyanobacteria, these other forms could also contribute to toxicity, highlighting the complexity of these ecosystems.

While elephants may have been more exposed to cyanotoxins due to their drinking behaviour (and the sheer quantity of water they consume daily), it is possible that other species were affected differently due to their drinking habits, which might have led them to ingest smaller quantities of cyanotoxins. The die-off occurred between March and May 2020, and the aerial survey was conducted in July 2020. The time gap between the event and the survey, coupled with the lack of ground-truthing, presents significant challenges in detecting the involvement of other species. Smaller carcasses would have been more susceptible to rapid scavenging and decomposition during this period. The survey might have been less effective in identifying smaller carcasses, especially in areas with dense vegetation. Additionally, high predation risks and the presence of scavengers in the region likely resulted in the quick removal of smaller carcasses[57–59]. The possibility that other species were affected but not detected due to these factors cannot be excluded, and this underscores the need for cautious interpretations.

The southern African region is projected to become drier and hotter [60,61], and pans across these regions will likely be subject to much shorter hydroperiods [62], with potential negative effects on water quantity and quality, and catastrophic repercussions on animals. In this context, the suggested distance covered by the elephants and the time passed after potential exposure to cyanotoxins not only shed light on this specific event but also represents the first steps in establishing a framework for investigating future mortality events of unknown causes in large mammals. This framework could be particularly crucial in regions experiencing drastic environmental changes. More efforts to improve mapping and further characterise pan ecohydrology are fundamental to understanding the implications of climate change on the ecology of the Okavango and other important ecosystems in the region, and beyond. We believe that the methods and findings of this study may serve future management and conservation strategies, providing a basis for addressing the challenges posed by changing environmental conditions. Integrating spatial analysis techniques in animal surveying could further serve as an early warning system to capture the onset and origin of animal mortality events, thereby offering a proactive approach to conservation. Developing a concurrent efficient sampling protocol that can be mobilised in response to or during these climatic and ecohydrological changes would add significant impact to early warning monitoring and management response strategies.

In conclusion, this unprecedented die-off within the largest remaining population of a threatened signature megafauna underlines the escalating concerns surrounding the impact of drought and climate change on the Okavango Delta, one of the most important ecosystems in the world. Globally, this event underscores the alarming trend of sudden, climate-induced diseases affecting large ungulates, reflecting the broader, devastating impacts of climate change on biodiversity and ecosystem health [63,64]. By establishing a methodological approach to tracking and analysing these events, our study contributes to the broader field of environmental science and animal conservation, providing critical insights that could help mitigate similar tragedies in the future.

Methods

Study Area

Our study focused on the eastern Okavango Panhandle region, the north-easternmost sector of the Okavango Delta, which comprises the concession areas NG11, NG12 and NG13 within the Ngamiland district, Botswana. The area is enclosed to the north, east and south by a border fence and veterinary fence, originally installed to prevent the transmission of zoonotic diseases to domestic animals, like the foot and mouth disease carried by buffalos [22] and Contagious Bovine Pleuropneumonia (CBPP) [23]. The west side of the eastern Panhandle is closed-off by the Okavango River where the water is relatively deeper and prevents non-aquatic animals from routinely crossing to either side [2]. The total extent of NG11, NG12 and NG13 concession areas within the veterinary fence and including the Okavango River is around 9268km^2. The climate of Botswana is classified as arid to semi-arid, and as such it is characterised by two distinct seasons. The wet season occurs between November and March, when total rainfall range between 300mm and 600mm per year. During the dry season between April and October, rainfall is virtually absent. Temperatures average between 15ºC and 27ºC, with peak low temperatures below 0ºC at night in winter (June to August), and peak high temperatures of over 40ºC during the day in summer (November to February) [65–67]. The elephant population in Botswana is currently the largest on Earth, counting over 132,000 individuals as of the latest report from the KAZA TFCA aerial survey[68]. The most updated published record of wildlife populations within the eastern Panhandle is from a dry season survey conducted in 2018, where over 15,000 elephants were estimated, alongside 25,000 cattle, 5,000 zebras, 4,500 goats and 500 wildebeest, to mention the most abundant animals [69]. Population estimates from past and current surveys in the Panhandle, however, show large fluctuations, but the trend has shown that the population has been increasing at around 9.5% a year [70]. Reasons for such high population increases is unknown, but could be due to high immigration and low emigration from and to other areas, population structure and recruitment rates, or climatic conditions such as response to droughts,

Datasets

Data were collected and analysed with permission of the Republic of Botswana Ministry of Environment, Nature Conservation and Tourism, research permit ENT 8/36/4 XLIX (11) and Ministry of Agriculture, research permit DVS 8/2/II (28).

Elephant survey data

We used locations of elephant carcasses and live animals from an aerial survey of the eastern Okavango Panhandle conducted by the Department of Wildlife and National Parks (DWNP) of Botswana and Ecoexist [71] in July 2020 following the reported elephant mass-mortality event[17]. The aerial survey, which employed the standard methodology of strip transect sampling [72], aimed to count the number of carcasses and live animals and estimate the age category of the carcasses. The survey used the standard classification method [24] to estimate the age of the carcasses (C1 to C4, fresh carcasses to very old bones) but adjusted based on local knowledge of carcasses decay in the region. The survey classified carcasses aged <1month as fresh (C1), carcasses aged <6months as recent (C2), and those aged >6months as bones [17].

Climate data

To assess the long-term climatic conditions in the eastern Panhandle, we obtained air temperature 2 m above ground between 2015 and 2023 from the ERA5 hourly re-analysis dataset provided by the European Centre for Medium-Range Weather Forecasts (ECMWF) at a resolution of 0.25º (~25km^2) [73]. We also obtained precipitation data from the TAMSAT dataset between 2015 and 2023, which comprises rainfall estimates based on satellite and ground-based observations for the African continent at 0.0375º resolution (~4 km^2) [74–76].

Water frequency data

The location of waterholes (pans) in the eastern Panhandle, was determined using an open-source water frequency product developed for the Kavango-Zambezi Transfrontier Conservation Area (KAZA) for the period 2017-2020 [77]. Sentinel-2 images and other remote sensing products were used to classify pixels within KAZA and isolate those classified as water, along with the frequency of classification.

Remote sensing data

Sentinel-2A/B Multi-Spectral Instrument Level-2A images (i.e., atmospherically, and geometrically corrected) between January 2019 and August 2023 were obtained from Google Earth Engine (GEE) using its python API. Since images prior 2019 were not available on GEE as Level-2A, individual cloud-free Sentinel-2 MSI Level-1C images between 2015 and 2018 were downloaded from CREODIAS data explorer online tool [78].

Remote sensing image processing

Sentinel-2A/B Multi-Spectral Instrument images available in GEE as Level-2A between 2019 and 2023 were filtered by cloud cover (60%) to avoid cloudy images, and pixels within each image were scanned through the *s2cloudless* algorithm [79] to mask out remaining cloud pixels and cloud shadow pixels within filtered images, discarding pixels with > 50% probability of cloud, and using the cloud shadow mask to remove likely shadow pixels. Images downloaded from CREODIAS were filtered for clouds and atmospherically corrected using the *Sen2Cor* atmospheric correction (AC) algorithm [80,81] to match the default image processing for Sentinel-2 images Level-2A by the European Space Agency (ESA).

Water frequency layer processing

Since the water frequency product contained all the pixels classified as water at least once within KAZA, we generated a custom region of interest (ROI) within the boundaries of the veterinary fence (i.e., eastern Okavango Panhandle) (Fig. 1) manually 'cropping out' the Okavango River and its north-eastern branching. The resultant ROI has an extent of 7,138 km^2. We excluded rivers and wetlands from the analysis to enhance the identification of an optimal threshold for the detection of pans, which would have been affected if perennial waters were included. The water frequency layer within the ROI was vectorised using QGIS Białowieża LTR v3.28.11, and the resultant product was a multi-polygon shapefile, where each polygon was the outline of single or group of contiguous pixels where water had been detected at least once between 2017 and 2020 [77].

Identification of Pans

To identify individual pans over time, we masked the atmospherically corrected Sentinel-2 images using the vectorised water frequency product mentioned above. This allowed to exclude from the images all the pixels that fell outside individual polygons, which were assumed to be land due to the nature of the product. Since pans recede during the dry season, hence not all pixels within these polygons were expected to always have water, we identified all remaining non-water pixels within the polygons for each image using the Automated Water Extraction Index (AWEI) [18] using the equation:

$$AWEI = \rho_{B2} + 2.5 \times \rho_{B3} - 1.5 \times (\rho_{B8} + \rho_{B11}) - 0.25 \times \rho_{B12}) \quad [1]$$

where ρ_{Bn} are Sentinel-2 bands blue (B2, 490 nm), green (B3, 560 nm), NIR (B8, 705 nm), SWIR1 (B11, 1610 nm) and SWIR2 (B12, 2190 nm), respectively. This version of AWEI we adopted is also referred to as $AWEI_{sh}$. This was originally formulated to improve shadow and dark pixels areas removal in non-urban environments, pushing all non-water pixels values below 0 and pulling water pixels above 0[18]. Yet, AWEI doesn't perform in the same way across the globe, and water pixels in this part of the world show much lower values (AWEI <= -0.2) [62]. We computed an optimal AWEI threshold to mask out remaining non-water pixel from those within the polygons using the Grey Histogram method [82], which uses the distribution of the input value (here AWEI) to generate classes, minimising variance within classes and maximising variance between classes. This method determined the point at which AWEI changed due to a change in classes (i.e., water/ non-water). We calculated the optimal AWEI threshold on the 95th percentile image between Mar and May of each year, aiming to capture water at its maximum extent between the end of the wet season and the beginning of the dry season, and further exclude potential false positives (previously undetected cloud pixels), and false negative (adjacent land effects). Individual AWEI thresholds for each year were averaged to account for potential errors introduced by different light, atmospheric conditions, and computation of AC across years, obtaining a final value of -0.3624 (rounded). The threshold was applied to all the images between 2015 and 2023, and each group of contiguous pixels within each polygon was considered as an individual pan. Including the main rivers and wetlands in the formulation of the threshold would have resulted in a much higher value due to the greater number of pixels detected in much clearer waters compared to pans, which tend to have higher AWEI. Using a higher threshold would have masked out most pans in the eastern Panhandle.

To ensure continuity of measurements over time and avoid likely gaps brought by cloud filtering, masking, and/ or absence of Sentinel-2 images, we grouped all threhsolded images bi-weekly, between the 1st and the 15th, and between the 15th and the last day of each month, using the 95th percentile. This resulted in two timestamps (i.e., observations) per month. Each group of contiguous pixels within each polygon in all 95th percentile images was collated to a dataset along with the latitude and longitude of its centroid, the count of contiguous pixels, and we extracted AWEI and the Normalised Difference Chlorophyll Index (NDCI)

[19] values at centroid. AWEI was used as a proxy of water availability, whereas NDCI was used as a proxy for phytoplankton biomass. NDCI was obtained using the equation:

$$NDCI = \frac{\rho_{B5} - \rho_{B4}}{\rho_{B5} + \rho_{B4}} \quad [2]$$

where ρ_{Bn} are Sentinel-2 bands near-infrared (B5, 705 nm) and red (B4, 665 nm), respectively.

Labelling pans

The final collated dataset comprised a total count of 128,667 pans between 2015 and 2023. This figure represents the aggregate count of observations, as pans were monitored multiple times (bi-weekly) during the analysis period. To discern individual water bodies, we assigned unique labels to distinguish between them based on their maximum observed extent, which was April 2021. This identification process resulted in the isolation of 3,389 distinct, or 'reference', pans from the cumulative observations. Each reference pan was defined by the centroid of its largest recorded extent and was surrounded by a 30 m radius buffer. We then matched the centroids of all recorded pan instances to these reference pan buffers at each timestamp. If a pan's centroid from any timestamp fell within this buffer, it was recognised as the same entity as the reference pan, thereby maintaining consistent identification despite potential shifts in centroid location due to changes in water levels. This methodological step ensures the accurate tracking of each unique pan over time, despite the repeated counting of the same pans across different timestamps, which initially led to the higher aggregate figure.

Location comparison between surveyed live and dead elephants

Due to the limited number of C1 carcasses points available from the 2020 aerial survey (*n=7*), C1 and C2 carcasses were combined into a single age category named *carcasses* (*n=161*). The other two categories were *bones* (*n=222*) and *live elephants* (*n=2682*). To understand if the way carcasses distributed across the eastern Panhandle differed from bones and live elephants, we computed the Nearest Neighbour Index (NNI) [83] using the equation:

$$\mathrm{NNI} = \frac{Observed\ Average\ Distance}{E[D]} \quad [3]$$

Where:

$$E[D] = \frac{1}{2\sqrt{\lambda}};\ \lambda = \frac{n}{A}$$

Here, n is the number of points and A is the area of the ROI. The $Observed\ Average\ Distance$ is the average of all the distances between each pair of points. The significance of NNIs was evaluated using a Monte Carlo simulation, which randomly permuted the locations of datapoints within the ROI to simulate complete spatial randomness (CSR) [84]. The Monte Carlo simulation was set to run for 999 iterations, ensuring both statistical robustness and computational efficiency. NNI was calculated for each simulated randomly distributed set of points at each iteration and compared to the observed points using a z-score to assess the degree to which the spatial pattern of the observed points deviated from a random distribution. A z-score beyond the range of 1.96 to -1.96 indicates the presence of statistically significant clusters. The z-score was obtained with the formula:

$$\mathrm{z_{score}} = \frac{Observed\ Average\ Distance - E[D]}{\sigma_{simulated}} \quad [4]$$

Where:

$$\sigma_{simulated} = \sqrt{\frac{\sum(x_{i,simulated} - \mu_{simulated})}{N_{simulated}}}$$

The points for each category were then crossed-compared to determine if their distributions differed statistically using the non-parametric two-sample Kolmogorov-Smirnov (KS) test, which makes use of every point in the samples irrespective of distribution and ordering [85].

Clusters identification

To further assess how carcasses, bones and live elephants distributed across the landscape, we determined the number of clusters that each category generated based on distances between points. The number of clusters in each category provided some indication on the spatial associations between points, such that fewer clusters may denote a higher likelihood of relationship between points. Clusters were determined using the DBSCAN method [86], that is a density-based algorithm that identifies within-group, distance-based clusters. DBSCAN uses an optimal average distance, referred to as *epsilon* and an arbitrary minimum number of points to generate clusters. The *epsilon* was automatically extracted from the data using an 'elbow method' algorithm, which sorted distances between points in ascending order and using a moving average identified the optimal value as the point at which distances increased sharply. The minimum number of points was set to 4 to prevent the formation of too small clusters.

Point pattern analysis

We determined which pans across the ROI elephants may have interacted with the most before dying by calculating the spatial autocorrelation between the locations of pans and the centre of each cluster for each category. Cluster centres were preferred to avoid noise brought by randomly distributed points, and to delineate areas that were common to spatially associated groups of carcasses and bones. To assess spatial autocorrelation, we used Local Moran's I [87], a statistic that we used to measure the similarity between neighbouring pans based on proximity to cluster centres. Given a set of n spatial units (i.e., the total number of pans for a given timestamp), and a variable x observed over these units (i.e., the distance between individual pans and the clusters centres), the Local Moran's I for the i^{th} unit (individual pans) is defined as:

$$I_i = \frac{n \cdot \sum_j w_{ij}(x_i - \bar{x})(x_j - \bar{x})}{2W \cdot S_0} \quad [5]$$

Where x_i and x_j are the distances of pans i and j to the nearest cluster centre, $\bar{x}$ is the mean distance across all pans, w_{ij} is the spatial weight, indicating whether *j* is neighbour of pan i or not. The denominator serves as a normalisation factor, where W represent the sum of spatial weights associated with a pan, reflecting its total 'neighbouring influence' or connectivity to other pans. This is doubled to account for the reciprocal nature of spatial relationships. S_0 is the global variance of pan-cluster centres distance. The spatial weights matrix was computed applying a k-Nearest Neighbour algorithm on the locations of the pans, where the optimal *k* was dynamically calculated as the number of pans within twice the average distance between all the pans [87]. This heuristic approach ensured that the spatial weights were drawn directly from the distribution of datapoints to avoid biasing the results, which may occur when setting a fixed *k* for areas of varying point density.

Reported animal intoxication and distances covered before death

To estimate the distance that elephants may have travelled between exposure to cyanotoxins and dying, we reviewed the literature to identify the typical elephant walking speeds, and the time between exposure to cyanobacteria and death in various animals. The literature suggested that elephants in the eastern

Panhandle walk an average of 4.5 km a day [25,27]. For the latter, the most relevant information were primarily extracted from the supplementary material in Wood (2016), which comprises of an extensive list of observations in published scientific literature between 1878 and 2012. In some instances, the link to cyanobacteria ingestion as cause of death was circumstantial and not proven by laboratory assessment, but with complementary empirical evidence, like observation of animal death after interaction with water covered in green/ blue-green substance at the water surface. Only observations with relatively specific timeframe of death were used. Descriptions like 'death within days' or 'died shortly after' were discarded, since they did not provide accurate enough time estimates. Conversely, death timeframes described as 'minutes', 'few hours', or 'several hours', were kept and arbitrarily assigned to 30 minutes, 6 hours, and 12 hours, respectively.

Standard Deviation Ellipses

Standard deviation ellipses (SDE) for each carcasses clusters were computed to identify their bivariate distribution (i.e., lat-long) and statistically summarise their dispersion and orientation[26]. Since SDE are built on the distribution of the data itself, they help to identify underlying spatial trends within typical confidence intervals drawn from a normal distribution. In other words, SDE allowed to identify areas where elephants were likely to have interacted, and these 'areas of interaction' were used to further filter out pans that may have not been visited by elephants before dying. SDE was computed using the centroid of carcasses clusters and the dispersion of datapoints to determine the directionality of the ellipses. SDE was calculated using the adapted ellipse equation:

$$\frac{(x-h)^2}{(p*\sigma_x)^2} + \frac{(y-k)^2}{(p*\sigma_y)^2} = 1 \qquad [6]$$

where:

$$h = \frac{1}{n}\sum_{i=1}^{n} x_i;\ k = \frac{1}{n}\sum_{i=1}^{n} y_i;$$

and:

$$\sigma_x = \sqrt{\frac{1}{n}\sum_{i=1}^{n}(x_i - h)^2};\ \sigma_y = \sqrt{\frac{1}{n}\sum_{i=1}^{n}(y_i - k)^2};$$

Here, n is the total number of points, x_i and y_i are the x and y coordinates of each point, respectively, h and k are the x and y coordinates of the mean points centre, respectively. The factor p determined how many standard deviations to consider when computing the width and height of the ellipse.

Acknowledgments

We would like to thank the Government of Botswana Ministry of Environment, Nature Conservation and Tourism, Ministry of Agriculture, Department of Wildlife and National Parks, and Department of Veterinary Services for granting permission for this research to take place, as well as providing data and resources. Thank you to all the team members involved in the research. Thank you to Natural Environmental Research Council (NERC) for providing funding for this research through Urgency grant NE/V013114/1, and the London NERC DTP grant NE/S007229/1, and thank you to the Elephant Crisis Fund, DWNP and Ecoexist for co-funding the elephant population survey. For the purpose of open access, the author has applied a Creative Commons Attribution (CC BY) license to any Author Accepted Manuscript version arising.

Data and code Availability

- The elephant survey data used in this study cannot be deposited in a public repository because it is owned by Ecoexist (https://www.ecoexistproject.org). To request access, contact info@ecoexistproject.org . Satellite data was obtained from Google Earth Engine, and available to those that signed up to the service (https://code.earthengine.google.com).
- Any additional information required to reanalyse the data reported in this paper, including the code, is available from the lead contact upon request.

Author contributions

Conceptualization: DL, EJT, ERM
Methodology: DL, EJT, NDB, ERM, GPM, ACS
Investigation: DL, EJT, NDB, MAC, AJ, ERM, SGHS
Visualization: DL
Supervision: EJT, MAC, AJ, DNS, SGHS
Writing—original draft: DL
Writing—review & editing: All Authors

Declaration of interests

Authors declare that they have no competing interests.

References

1. Barton, P. S., Reboldi, A., Bonat, S., Mateo-Tomás, P. & Newsome, T. M. Climate-driven animal mass mortality events: is there a role for scavengers? *Envir. Conserv.* **50**, 1–6 (2023).
2. Van Aarde, R. J., Pimm, S. L., Guldemond, R., Huang, R. & Maré, C. The 2020 elephant die-off in Botswana. *PeerJ* **9**, e10686 (2021).
3. Pozo, R. A., Coulson, T., McCulloch, G., Stronza, A. L. & Songhurst, A. C. Determining baselines for human-elephant conflict: A matter of time. *PLoS ONE* **12**, e0178840 (2017).
4. Maron, D. F. What's killing Botswana's elephants? Here are the top theories. https://www.nationalgeographic.com/animals/article/botswana-elephant-death-mystery (2020).
5. Azeem, S., Bengis, R., Van Aarde, R. & Bastos, A. D. S. Mass Die-Off of African Elephants in Botswana: Pathogen, Poison or a Perfect Storm? *African Journal of Wildlife Research* **50**, (2020).
6. Benza, B. Botswana says toxins in water killed hundreds of elephants. https://www.reuters.com/article/us-botswana-elephants-idUSKCN26C0WA/ (2020).
7. Huisman, J. *et al.* Cyanobacterial blooms. *Nat Rev Microbiol* **16**, 471–483 (2018).
8. Paerl, H. W. & Otten, T. G. Harmful Cyanobacterial Blooms: Causes, Consequences, and Controls. *Microb Ecol* **65**, 995–1010 (2013).
9. Hou, X. *et al.* Global mapping reveals increase in lacustrine algal blooms over the past decade. *Nat. Geosci.* **15**, 130–134 (2022).
10. Wood, R. Acute animal and human poisonings from cyanotoxin exposure — A review of the literature. *Environment International* **91**, 276–282 (2016).
11. Svirčev, Z. *et al.* Global geographical and historical overview of cyanotoxin distribution and cyanobacterial poisonings. *Arch Toxicol* **93**, 2429–2481 (2019).
12. Matthews, M. W., Bernard, S. & Winter, K. Remote sensing of cyanobacteria-dominant algal blooms and water quality parameters in Zeekoevlei, a small hypertrophic lake, using MERIS. *Remote Sensing of Environment* **114**, 2070–2087 (2010).

13. Dalu, T. & Wasserman, R. J. Cyanobacteria dynamics in a small tropical reservoir: Understanding spatio-temporal variability and influence of environmental variables. *Science of The Total Environment* **643**, 835–841 (2018).
14. Bengis, R. *et al.* Eco-epidemiological and pathological features of wildlife mortality events related to cyanobacterial bio-intoxication in the Kruger National Park, South Africa. *J. S. Afr. Vet. Assoc.* **87**, (2016).
15. Veerman, J., Kumar, A. & Mishra, D. R. Exceptional landscape-wide cyanobacteria bloom in Okavango Delta, Botswana in 2020 coincided with a mass elephant die-off event. *Harmful Algae* **111**, 102145 (2022).
16. Foggin, C. M. *et al.* Pasteurella sp. associated with fatal septicaemia in six African elephants. *Nat Commun* **14**, 6398 (2023).
17. Songhurst, A. & Tsholofelo, C. *Elephant Population and Carcass Survey Report. Okavango Panhandle, Botswana (NG10, NG11, NG12 and NG13)*. 38 (2020).
18. Feyisa, G. L., Meilby, H., Fensholt, R. & Proud, S. R. Automated Water Extraction Index: A new technique for surface water mapping using Landsat imagery. *Remote Sensing of Environment* **140**, 23–35 (2014).
19. Mishra, S. & Mishra, D. R. Normalized difference chlorophyll index: A novel model for remote estimation of chlorophyll-a concentration in turbid productive waters. *Remote Sensing of Environment* **117**, 394–406 (2012).
20. Hart, R. C. A LIMNOLOGICAL PROFILE OF THE UPPER OKAVANGO DELTA AT LOW WATER LEVEL. *Southern African Journal of Aquatic Sciences* **23**, 21–33 (1997).
21. Msiteli-Shumba, S., Kativu, S., Utete, B., Makuwe, E. & Hulot, F. D. Driving factors of temporary and permanent shallow lakes in and around Hwange National Park, Zimbabwe. *WSA* **44**, (2018).
22. Perkins, J. S. 'Only connect': Restoring resilience in the Kalahari ecosystem. *Journal of Environmental Management* **249**, 109420 (2019).
23. Marobela, C. Contagious bovine pleuropneumonia in Botswana: experience with control, eradication, prevention and surveillance. *Vet Ital* **47**, (2011).
24. Douglas-Hamilton, I. & Burrill, A. USING ELEPHANT CARCASS RATIOS TO DETERMINE POPULATION TRENDS. (1991).
25. Vogel, S. M. *et al.* Exploring movement decisions: Can Bayesian movement-state models explain crop consumption behaviour in elephants (*Loxodonta africana*)? *Journal of Animal Ecology* **89**, 1055–1068 (2020).
26. Wang, B., Shi, W. & Miao, Z. Confidence Analysis of Standard Deviational Ellipse and Its Extension into Higher Dimensional Euclidean Space. *PLoS ONE* **10**, e0118537 (2015).
27. Loarie, S. R., Aarde, R. J. V. & Pimm, S. L. Fences and artificial water affect African savannah elephant movement patterns. *Biological Conservation* **142**, 3086–3098 (2009).
28. African News Agency. Botswana probes mysterious death of 56 elephants. https://www.iol.co.za/news/africa/botswana-probes-mysterious-death-of-56-elephants-48239310 (2020).
29. Pozo, R. A. *et al.* Elephant space-use is not a good predictor of crop-damage. *Biological Conservation* **228**, 241–251 (2018).
30. Naidoo, R. *et al.* Mapping and assessing the impact of small-scale ephemeral water sources on wildlife in an African seasonal savannah. *Ecological Applications* **30**, (2020).
31. Songhurst, A. & Coulson, T. Exploring the effects of spatial autocorrelation when identifying key drivers of wildlife crop-raiding. *Ecol Evol* **4**, 582–593 (2014).
32. Songhurst, A. Measuring human–wildlife conflicts: Comparing insights from different monitoring approaches. *Wildl. Soc. Bull.* **41**, 351–361 (2017).
33. Schlossberg, S., Chase, M. J. & Sutcliffe, R. Evidence of a Growing Elephant Poaching Problem in Botswana. *Current Biology* **29**, 2222-2228.e4 (2019).
34. Roever, C. L., Van Aarde, R. J. & Chase, M. J. Incorporating mortality into habitat selection to identify secure and risky habitats for savannah elephants. *Biological Conservation* **164**, 98–106 (2013).
35. Haynes, G. Longitudinal studies of african elephant death and bone deposits. *Journal of Archaeological Science* **15**, 131–157 (1988).
36. Ramberg, L., Wolski, P. & Krah, M. Water balance and infiltration in a seasonal floodplain in the Okavango Delta, Botswana. *Wetlands* **26**, 677–690 (2006).
37. Welch, E. B. & Cooke, G. D. Internal Phosphorus Loading in Shallow Lakes: Importance and Control. *Lake and Reservoir Management* **21**, 209–217 (2005).

38. Krah, M. *et al.* Nutrient Budget in the Seasonal Wetland of the Okavango Delta, Botswana. *Wetlands Ecol Manage* **14**, 253–267 (2006).
39. Richer, R., Banack, S. A., Metcalf, J. S. & Cox, P. A. The persistence of cyanobacterial toxins in desert soils. *Journal of Arid Environments* **112**, 134–139 (2015).
40. Cirés, S., Casero, M. & Quesada, A. Toxicity at the Edge of Life: A Review on Cyanobacterial Toxins from Extreme Environments. *Marine Drugs* **15**, 233 (2017).
41. Chatziefthimiou, A. D., Banack, S. A. & Cox, P. A. Biocrust-Produced Cyanotoxins Are Found Vertically in the Desert Soil Profile. *Neurotox Res* **39**, 42–48 (2021).
42. Veerman, J., Mishra, D. R., Kumar, A. & Karidozo, M. Environmental drivers behind the exceptional increase in cyanobacterial blooms in Okavango Delta, Botswana. *Harmful Algae* **137**, 102677 (2024).
43. Merel, S. *et al.* State of knowledge and concerns on cyanobacterial blooms and cyanotoxins. *Environment International* **59**, 303–327 (2013).
44. Oberholster, P. J., Botha, A. M. & Botha, J. G. Linking climate change and progressive eutrophication to incidents of clustered animal mortalities in different geographical regions of South Africa. *Afr. J. Biotechnol.* **8**, 5825–5832 (2009).
45. Sikes, S. K. *The Natural History of the African Elephant*. (Weidenfeld & Nicolson, London, 1971).
46. *Biology, Medicine, and Surgery of Elephants*. (Blackwell Pub, Ames, Iowa, 2006).
47. Dunkin, R. C., Wilson, D., Way, N., Johnson, K. & Williams, T. M. Climate influences thermal balance and water use in African and Asian elephants: physiology can predict drivers of elephant distribution. *Journal of Experimental Biology* **216**, 2939–2952 (2013).
48. *Toxic Cyanobacteria in Water: A Guide to Their Public Health Consequences, Monitoring and Management*. (CRC Press, Boca Raton London New York, 2021).
49. Nonga, H. E. *et al.* Possible involvement of microcystins in the unexplained mass mortalities of Lesser Flamingo (Phoeniconaias minor Geoffroy) at Lake Manyara in Tanzania. *Hydrobiologia* **678**, 167–178 (2011).
50. Corfield, T. F. Elephant mortality in Tsavo National Park, Kenya. *African Journal of Ecology* **11**, 339–368 (1973).
51. Wato, Y. A. *et al.* Prolonged drought results in starvation of African elephant (Loxodonta africana). *Biological Conservation* **203**, 89–96 (2016).
52. Ndlovu, M. *et al.* Age-sex structure of drought-driven African elephant (Loxodonta africana) mortality in Hwange National Park, Zimbabwe. *Scientific African* **19**, e01459 (2023).
53. Evans, A. M. *et al.* Nitrogen fixation by Baltic cyanobacteria is adapted to the prevailing photon flux density. *New Phytologist* **147**, 285–297 (2000).
54. Gao, Y., O'Neil, J., Stoecker, D. & Cornwell, J. Photosynthesis and nitrogen fixation during cyanobacteria blooms in an oligohaline and tidal freshwater estuary. *Aquat. Microb. Ecol.* **72**, 127–142 (2014).
55. Wang, H. *et al.* From unusual suspect to serial killer: Cyanotoxins boosted by climate change may jeopardize megafauna. *The Innovation* **2**, 100092 (2021).
56. Bouma-Gregson, K., Kudela, R. M. & Power, M. E. Widespread anatoxin-a detection in benthic cyanobacterial mats throughout a river network. *PLoS ONE* **13**, e0197669 (2018).
57. Schiess-Meier, M., Ramsauer, S., Gabanapelo, T. & König, B. Livestock Predation—Insights From Problem Animal Control Registers in Botswana. *J Wildl Manag* **71**, 1267–1274 (2007).
58. Kesch, M. K., Bauer, D. T. & Loveridge, A. J. Break on Through to the Other Side: The Effectiveness of Game Fencing to Mitigate Human—Wildlife Conflict. *African Journal of Wildlife Research* **45**, 76 (2015).
59. Selebatso, M., Fynn, R. & Maude, G. Adaptive activity patterns of a blue wildebeest population to environmental variability in fragmented, semi-arid Kalahari, Botswana. *Journal of Arid Environments* **136**, 15–18 (2017).
60. Engelbrecht, F. *et al.* Projections of rapidly rising surface temperatures over Africa under low mitigation. *Environ. Res. Lett.* **10**, 085004 (2015).
61. Nangombe, S. *et al.* Record-breaking climate extremes in Africa under stabilized 1.5 °C and 2 °C global warming scenarios. *Nature Clim Change* **8**, 375–380 (2018).
62. Schaffer-Smith, D. *et al.* Tracking a blue wave of ephemeral water across arid southern Africa. *Environ. Res. Lett.* **17**, 114063 (2022).

63. Kutz, S. *et al.* Erysipelothrix rhusiopathiae associated with recent widespread muskox mortalities in the Canadian Arctic. **56**, (2015).
64. Kock, R. A. *et al.* Saigas on the brink: Multidisciplinary analysis of the factors influencing mass mortality events. *Sci. Adv.* **4**, eaao2314 (2018).
65. Byakatonda, J., Parida, B. P. & Kenabatho, P. K. Relating the dynamics of climatological and hydrological droughts in semiarid Botswana. *Physics and Chemistry of the Earth, Parts A/B/C* **105**, 12–24 (2018).
66. Nkemelang, T., New, M. & Zaroug, M. Temperature and precipitation extremes under current, 1.5 °C and 2.0 °C global warming above pre-industrial levels over Botswana, and implications for climate change vulnerability. *Environ. Res. Lett.* **13**, 065016 (2018).
67. Akinyemi, F. O. & Abiodun, B. J. Potential impacts of global warming levels 1.5 °C and above on climate extremes in Botswana. *Climatic Change* **154**, 387–400 (2019).
68. Bussière, E. M. S. & Potgieter, D. *KAZA Elephant Survey 2022, Volume I: Results and Technical Report, KAZA TFCA Secretariat, Kasane, Botswana.* (2023).
69. Chase, M., Schlossberg, S., Sutcliffe, R. & Seonyatseng, E. DRY SEASON AERIAL SURVEY OF ELEPHANTS AND WILDLIFE IN NORTHERN BOTSWANA. (2018).
70. Songhurst, A., Chase, M. & Coulson, T. Using simulations of past and present elephant (Loxodonta africana) population numbers in the Okavango Delta Panhandle, Botswana to improve future population estimates. *Wetlands Ecol Manage* **23**, 583–602 (2015).
71. Ecoexist. THE ECOEXIST PROJECT: Reducing conflict and fostering coexistence between elephants and people. https://www.ecoexistproject.org (2023).
72. Norton-Griffiths, M. Counting Animals. (1978).
73. Hersbach, H. *et al.* ERA5 hourly data on single levels from 1940 to present. Copernicus Climate Change Service (C3S) Climate Data Store (CDS). https://doi.org/10.24381/cds.adbb2d47 (2023).
74. Maidment, R. I. *et al.* The 30 year TAMSAT African Rainfall Climatology And Time series (TARCAT) data set. *J. Geophys. Res. Atmos.* **119**, (2014).
75. Tarnavsky, E. *et al.* Extension of the TAMSAT Satellite-Based Rainfall Monitoring over Africa and from 1983 to Present. *JOURNAL OF APPLIED METEOROLOGY AND CLIMATOLOGY* **53**, (2014).
76. Maidment, R. I. *et al.* A new, long-term daily satellite-based rainfall dataset for operational monitoring in Africa. *Sci Data* **4**, 170063 (2017).
77. Swift, M., Schaffer-Smith, D. & Killea, A. Map of surface water frequency observed 2017-2020, Schaffer-Smith et al 2022. https://doi.org/10.4211/hs.6f5b34803dc247e890925d7f26b04a3b (2022).
78. CREODIAS. CREODIAS. https://explore.creodias.eu (2023).
79. Braaten, J. Sentinel-2 Cloud Masking with s2cloudless. https://developers.google.com/earth-engine/tutorials/community/sentinel-2-s2cloudless (2023).
80. ESA. *Sen2Cor Software Release Note*. http://step.esa.int/thirdparties/sen2cor/2.9.0/docs/S2-PDGS-MPC-L2A-SRN-V2.9.0.pdf (2020).
81. ESA. Sen2Cor v2.9. https://step.esa.int/main/snap-supported-plugins/sen2cor/sen2cor-v2-9/ (2020).
82. Otsu, N. A Threshold Selection Method from Gray-Level Histograms. *IEEE Trans. Syst., Man, Cybern.* **9**, 62–66 (1979).
83. Diggle, P. J. *Statistical Analysis of Spatial and Spatio-Temporal Point Patterns*. (Chapman and Hall/CRC, 2013). doi:10.1201/b15326.
84. Kroese, D. P., Brereton, T., Taimre, T. & Botev, Z. I. Why the Monte Carlo method is so important today. *WIREs Computational Stats* **6**, 386–392 (2014).
85. Lopes, R. H. C., Reid, I. & Hobson, P. R. The two-dimensional Kolmogorov-Smirnov test. (2007).
86. Ester, M., Kriegel, H.-P. & Xu, X. A Density-Based Algorithm for Discovering Clusters in Large Spatial Databases with Noise. (1996).
87. Anselin, L. Local Indicators of Spatial Association-LISA. *Geographical Analysis* **27**, 93–115 (1995).